The Effect of Thermal and Electrical Conductivities on the Ablation Volume during Radiofrequency Ablation Process

Mohammed S. Ahmed[1], Mohamed Tarek El-Wakad[2], Mohammed A. Hassan[3]
Department of Biomedical Engineering-Faculty of Engineering, Helwan University, Cairo, Egypt[1]
Department of Biomedical Engineering-Faculty of Engineering & Technology, Future University in Egypt, Cairo, Egypt[2]
Department of Biomedical Engineering-Faculty of Engineering, Helwan University, Cairo, Egypt[3]

***Abstract*—Radiofrequency ablation (RFA) is the treatment of choice for certain types of cancers, especially liver cancer. However, the main issue with RFA is that the larger the tumor volume, the longer the ablation period. That causes more pain for the patient, so the surgeons perform a larger number of ablation sessions or surgeries. The current commonly used electrode material, nickel-titanium alloy, used in RFA is characterized by low thermal and electrical conductivities. Using an electrode material with higher electrical conductivity and thermal conductivity provides more thermal energy to tumors. In this paper, we design two models: a cool-tip RF electrode and a multi-hook RF electrode, which aim to study the effect of the thermal and electrical conductivities of the electrode material on ablation volume. Gold, silver, and platinum have higher thermal and electrical conductivity than nickel and titanium alloy, and therefore we studied the effect of these materials on the ablation volume using two different designs, which are the RF cooling tip electrode and the multi-hook electrode. The proposed model reduces the ablation time and damages healthy tissue while increasing the ablation volume with values ranging from 2.6 cm^3 to 15.4 cm^3. The results show ablation volume increasing with materials characterized by higher thermal and electrical conductivities and thus reducing patient pain.**

Keywords*—Radiofrequency ablation (RFA); finite element method (FEM); COMSOL; Cool-tip RF electrode; multi-hooks electrode; large tumor ablation

I. Introduction

Cancer is one of the leading causes of death in both men and women, with 11.3 million deaths in 2020 [1]. The second most common cause of death in Egypt [2]. Liver cancer is the fourth most common type of cancer worldwide [3] and the second most common cancer in Egypt [2]. The most common way to treat liver tumors is resection (RES), microwave ablation (MWA), and radiofrequency ablation (RFA) [4]. RFA is based on passing high-frequency (400-500 kHz) electric currents through the tissue between two excitation electrodes, causing the tissues to heat up, which results in tissue ablation [5, 6]. The main limitation with RFA is that as tumor volume increases the whole-tumor ablation duration increases, which the patient's pain. Therefore, RFA is effective for small tumors (i.e., tumors with a diameter of 3 cm), but still not very effective for large tumors [7, 8]. Radiofrequency (RF) electrode materials should be biocompatible with the human body and have low relative permittivity to be compatible with any device [9, 10]. Fang et al., suggested several factors contribute to increased ablation volume with reduced ablation time, such as electrode design and the material of the electrode [11]. Electrodes made of materials with high thermal conductivity and high electrical conductivity can contribute to increased ablation volume and reduced time of ablation [12, 13]. Current electrode materials used in RFA are characterized by low thermal and electrical conductivity, such as nickel-titanium alloy [14].

The finite element model (FEM) is a numerical technique used to perform finite element analysis (FEA) of any given physical phenomenon [15]. Alemayehu, et al., have simulated a medical problem about bones and joints using FEM to solve the problems of cartilage erosion [16]. In [17], the authors have used FEM in various fields of dentistry for calculating the strength and behavior of structures and have succeeded in calculating deflection, stress, vibration, and buckling behavior. While on the other side, the authors simulated FEM to ablate breast cancer by using RFA and succeeded in abating 80% of the tumor [18]. In [19], the authors designed FEM to ablate liver tumors by using cool-tip RF electrodes.

Many studies are conducted in ex-vivo studies [20, 21] and clinical studies [22, 23] on the effect of electrode materials on volume ablation due to their electrical and thermal properties. Thermal conductivity gets high attention for researchers in theory because, as the thermal conductivity of the material increases, so the thermal emission capacity of the material does [24, 25]. Several theoretical studies compared materials that have high thermal conductivity with those of low thermal conductivity [26, 27], while other several studies compared materials that have high electrical conductivity with those that have low electrical conductivity [28-30]. These studies found that the use of materials of high thermal and electrical conductivities helps to increase the ablation volume while reducing the ablation time.

The aim of this paper is to study the effect of different materials having high thermal conductivity and high electrical conductivity for RF electrodes on the ablation volume using a FEM. Although our results are specific to the case of RFA of the liver, they may also be important for other ablation applications, such as kidney cancer. In this paper, we design two models based on the cool tip RF electrode and the multi-hook RF electrode.

The two models are based on a numerical finite element analysis to compute the distribution of heat and electric potential inside the damaged and surrounding tissue during an RF ablation. These two models simulate the ablation of large tumors while trying to reduce the damage to healthy cells in less time. This paper is organized as follows: First, an explanation of the methodology of the proposed model, including its equations. Second, the results and discussions of the proposed model show the differences in results between our model and others, and finally, the conclusions.

II. METHODS

We used COMSOL 5.4 software [31] to implement FEM to develop two models (cool-tip and multi-hook RF electrode models). Each model is included within a cylindrical domain that contains both the liver domain and an electrode domain. The radius of the base of the cylinder is 5 cm, and the height is 12 cm.

A. FEM Modeling

1) Liver domain: The liver tissue is the main tissue capable of generating glucose from lactate, glycerol, and amino acids (mainly alanine from muscle). It is located in the right upper quadrant of the abdominal cavity, rests just below the diaphragm, to the right of the stomach, and overlies the gallbladder. The liver domain includes everything surrounding the electrode: blood, blood vessels, and liver tissues.

2) Electrode domains

a) A cool-tip RF electrode domain: It is distinguished by its excellent resistance to rust and corrosion as well as by its high flexibility, which avoids breakage or distortion, both of which pose risks to the patient's safety. The proposed model disregards the inner tube for brine injection responsible for cooling.

The cool tip RF electrode domain, consists of an electrode domain and a trocar domain as shown in Fig. 1 [32].

The RF electrode consists of:

- An insulated stainless-steel trocar with a diameter of 0.73 mm and a height of 12 cm.
- A nickel-titanium alloy (nitinol) electrode with a height of 3 cm and a diameter of 0.73 mm with a tip in a cone.

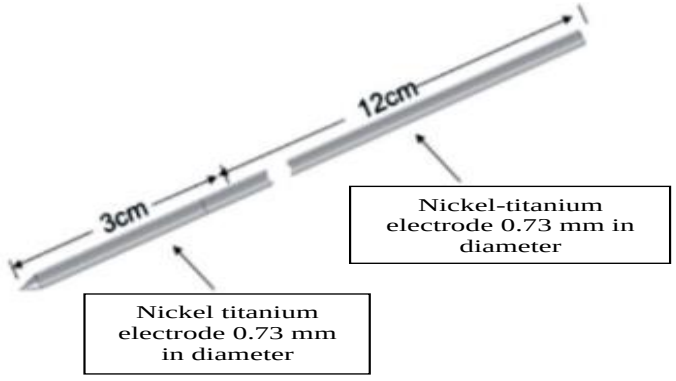

Fig. 1. A simplified model shows the design of the electrode [32].

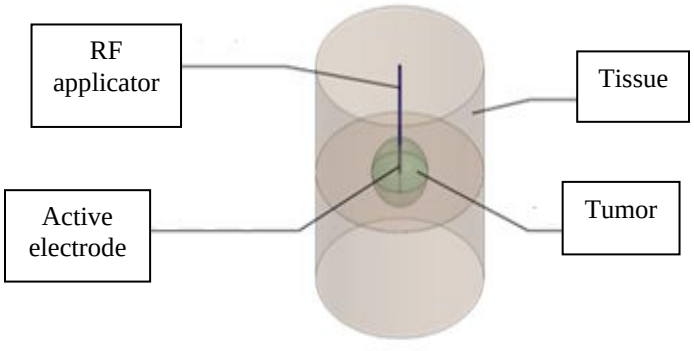

Fig. 2. A simple model that shows how a RF electrode works to ablate the tumor.

Fig. 2 explains the issue, where the tissue area is modelled as a cylindrical volume with the active electrode inserted into the tissue. The tissue area consists of the tumor in a spherical shape surrounded by healthy tissue inside the cylinder.

In our study, we set the power equal to 15 watts and assumed that the tumor was spherical, as 56% of liver cancer patients had spherical tumors [33]. We also assumed that the tumor size was 16 cm^3, which is the largest volume that has been recorded for a liver tumor in Egypt in the last ten years [34].

a) A multi-hook RF electrode domain

Fig. 3 shows the design of multi-hook electrodes.

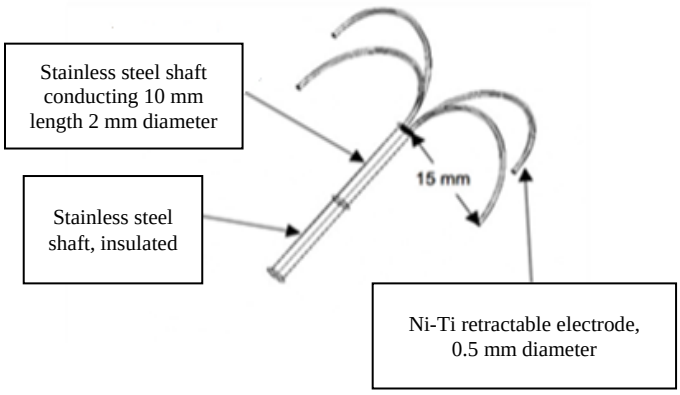

Fig. 3. Simplified model shows design of the electrode.

The multi-hook RF electrode consists of:

- Insulated stainless steel trocar with a height of 10 cm and a diameter of 2 mm.
- A stainless-steel electrode measures 1 cm in height and 2 mm in diameter, with a nickel-titanium alloy with a 1.5 cm major diameter and 0.5 mm minor diameter tip in a hook.

In our model, the initial conditions and boundary conditions of the simulation model are defined. We set the multi-hook RF electrode as the voltage source and set power equal to 15 watts, while we defined the liver boundary as the ground.

3) Thermal and electrical properties: Table I lists the different properties at 500 kHz used in our model to describe the gold (Au), the silver (Ag), the platinum (Pt), the nickel-titanium alloy (Nitinol), artery wall, and blood. The table shows the relative permittivity, density, and melting point values of the materials in the table are close. On the other hand, the table shows a clear variance in thermal and electrical conductivity values. So, we chose these two characteristics to study their effect on the ablation volume. During the ablation process, the tissue temperature increases. Changes in temperature lead to changes in the electrical conductivity of biological tissues [35]. The changes that occurred in the electrical conductivity of the tissues within the model are described as follows:

$$\delta(T) = \delta_{\circ}[1 + k_1 \Delta T] \quad (1)$$

where:

$\delta_{\circ}$ is the initial electrical conductivity at the reference temperature (30℃), k_1 is the temperature coefficient, ΔT [℃] is the temperature difference from the initial reference temperature.

The linear electrical conductivity of the model is determined by.

$$\delta(T) = 0.155[1 + 0.0265\Delta T] \quad (2)$$

Expect the artery wall, and the equation is.

$$\delta(T) = 0.221[1 + 0.0265\Delta T] \quad (3)$$

Both equations are bounded at 30–80℃.

4) Mathematical equations

a) Electric field: The electro-magnetic problem has been solved using a simplified version of Maxwell's equation that uses the quasistatic approximation because the displacement current is so minimal relative to the resistive current at the frequency range employed in the RFA technique (450–550 kHz). As a result, the generalized Laplace equation has been used to calculate the electric field.

$$\nabla.(\sigma \Delta V) = 0 \quad (4)$$

Where:

σ is (S/m) the electrical conductivity and V is the electric potential (V). The current study takes into account the tissue's electrical conductivity, which is temperature-dependent and increases linearly (10% per °C).

In the model tissues, the losses due to heat contact with the tissues are not significant, so we neglected the losses in our model [39]. The electric field E (V/m) is calculated from the equation.

$$E = -\nabla V \quad (5)$$

where $\boldsymbol{\nabla}$ is the operating factor. Then, current density J (A/m^2) is calculated from

$$J = E/\rho e \quad (6)$$

where ρe is the electrical resistivity of the material (Ω m)

b) Bioheat equation: Calculations of the temperature distributions were made using FEM. By resolving the heat transfer equation (Equation 7), where we ignored the metabolic heat production Q_m and blood perfusion heat loss Q_b due to their comparatively small magnitudes, we were able to determine the temperature distribution throughout the tissue:

Bioheat transfer due to RF current can be mathematically explained by the following Pennes equation [40].

$$\rho c\, \partial T/\partial t = \nabla \cdot (k \nabla T) - \rho_b c_b \omega_b (T - T_b) + Q_m + JE + Q_b \quad (7)$$

$$JE = \sigma |\nabla V^2| \quad (8)$$

$$Q_b = \omega_b c_b (T_b - T) \quad (9)$$

where ρ is the density of tissue (kg/m^3), c is the specific heat capacity of the tissue (J/kg/K), k is the tissue thermal conductivity (W/m/K), ω_b is the blood perfusion rate (1/s), Q_m is the volumetric heat produced by the metabolism (W/m^3), JE is joule heating that represents heat generated from RF, where is the density of current, E is the intensity of the electric field,σ is the conductivity with a unit of Sm^{-1}, V is the voltage impressed on the electrode, Q_b is the volumetric heat produced by radiofrequency heating (Wm^{-3}) calculated using Equation (2), T_b is the core blood temperature (supposed to be 37°C), because the blood vessels effect was discarded in this study then we can assume T_b and T are equal then $Q_b$was set to zero Wm^{-3}

c) Boundary conditions

The boundary conditions are:

temp = normal body temperature (37 °C)

voltage = 0 V.

TABLE I. DIFFERENT PROPERTIES OF THE MODEL [36-38]

Material	Electrical conductivity σ (S/m)	Thermal conductivity (W/ m. K)	Relative permittivity (ε_r)	Density (kg/m3)	Melting point (℃)
Gold (Au)	44.2×10^6	315	1.143	1060	1064
Silver (Ag)	62.1×10^6	429	1.2	999	961.8
Platinum (Pt)	9.3×10^6	69.1	2.7	2190	1768
Nickel-titanium alloy (Nitinol)	2.4×10^6	18	86	6450	1650
Normal liver tissues	0.333	0.512	44.9	1060	-
Normal tumor tissues	0.1168	0.552	60.2	999	-

The complete FEM model's initial voltage and temperature have been taken into account to be 0 V and 37°C, respectively. The cylinder domain's bottom surface has been adjusted to 0 V to mimic a dispersive ground pad.

In the FEM model, an RF generator-controlled variable voltage source has been added to the electrode borders. All of the FEM model's remaining outside boundaries has been subjected to an electrical insulation boundary condition. For ten minutes, all of the numerical simulations of temperature-controlled RFA in various tissues were run. Furthermore, multiple temperature values were ranging from 50°C to 60°C.

d) Ablated tissue: The ablation area (i.e., where cell death occurs), it depends on the following factors:

- Damage time is the amount of time required to destroy the tumor-infected, damaged cell, equaling 10 minutes.
- The ablated temperature, equal to 50 °C, is the temperature required to destroy tumor-infected, damaged cells.
- Enthalpy change is the amount of heat evolved or absorbed in liver tissues (0 J/kg).

III. Results and Discussion

Cool-tip RF electrodes and multi-hook electrode ablation in our study depended on three materials: gold, silver, and platinum. This study analyzed these materials to provide guidance in clinical practice.

A. Cool-tip RF Electrode

Table II shows the ablation volumes due to the used electrode materials at different ablation durations.

TABLE II. Results from Simulation with a Cool-tip RF Electrode

Time (min)	Electrode material	Ablation volume(cm^3)
1	Nitinol	2.5
	Pt	4.7
	Ag	6.4
	Au	7.6
2.5	Nitinol	3.7
	Pt	6..8
	Ag	8.4
	Au	9.5
5	Nitinol	5.1
	Pt	8.4
	Ag	10.1
	Au	11.3
7.5	Nitinol	6.2
	Pt	10.3
	Ag	12
	Au	13.3
10	Nitinol	7.4
	Pt	12.2
	Ag	13.9
	Au	15.2

The ablation volume of tumor results output from gold, silver, platinum, nickel-titanium alloys, and electrodes respectively is shown in Fig. 4, 5, 6, and 7, respectively.

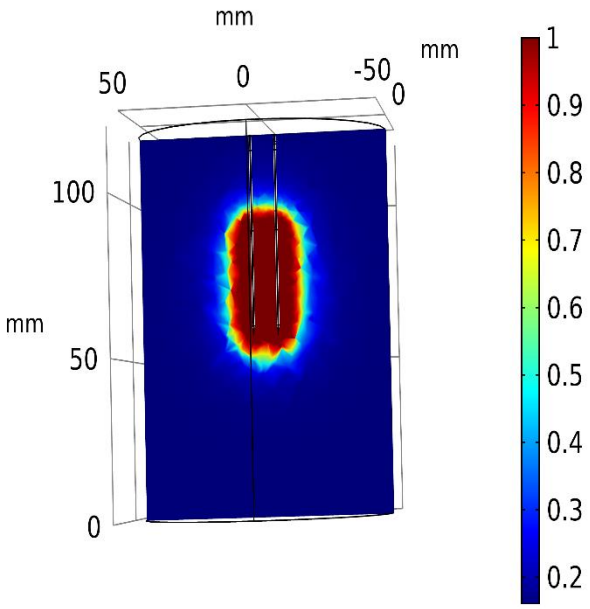

Fig. 4. View of the fraction of damage and the ablation volume resulting from using a cool-tip RF electrode made of Gold after ten minutes.

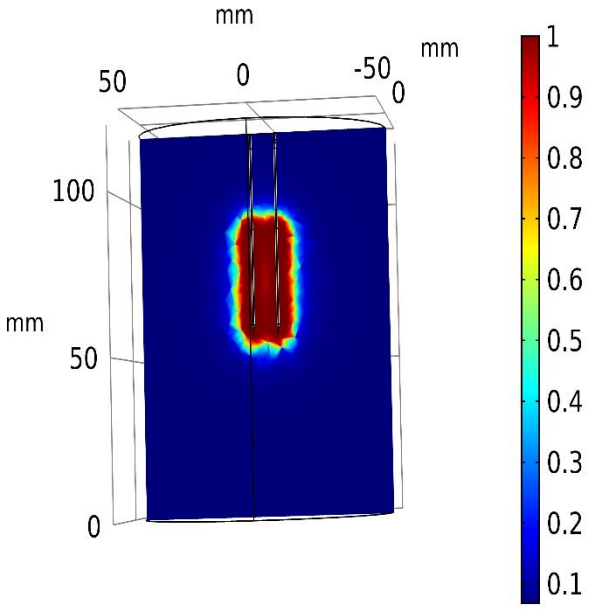

Fig. 5. View of the fraction of damage and the ablation volume resulting from using a cool-tip RF electrode made of Silver after ten minutes.

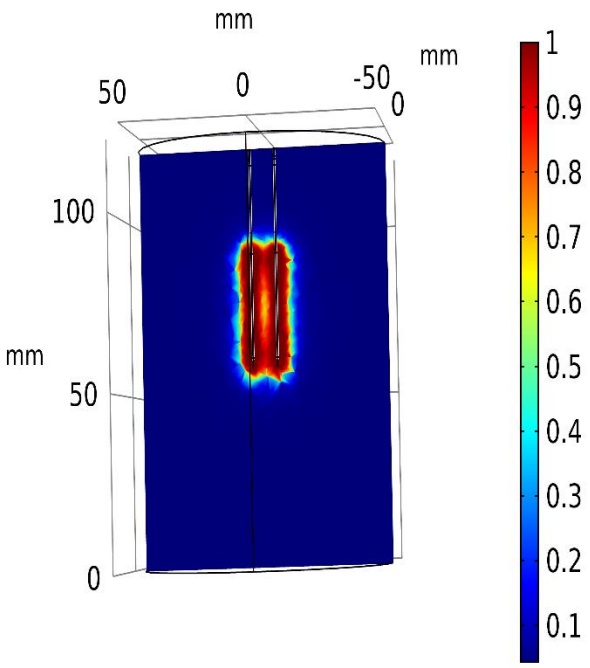

Fig. 6. View of the fraction of damage and the ablation volume resulting from using a cool-tip RF electrode made of Platinum after ten minutes.

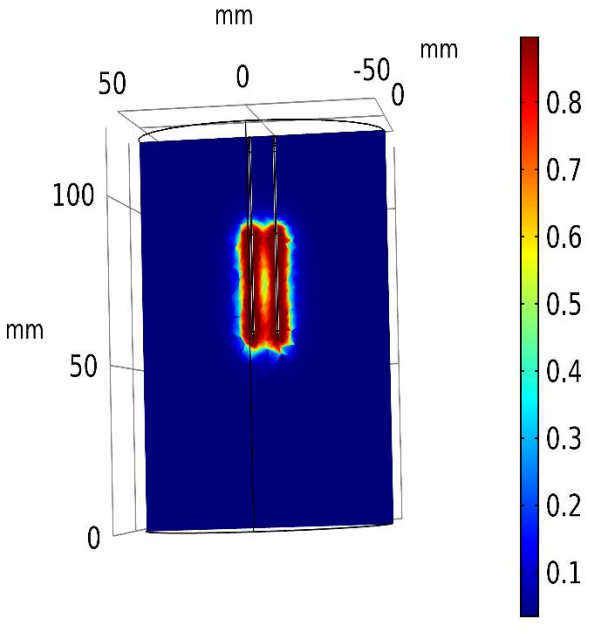

Fig. 7. View of the fraction of damage and the ablation volume resulting from using a cool-tip RF electrode made of Nickel-Titanium alloy after ten minutes.

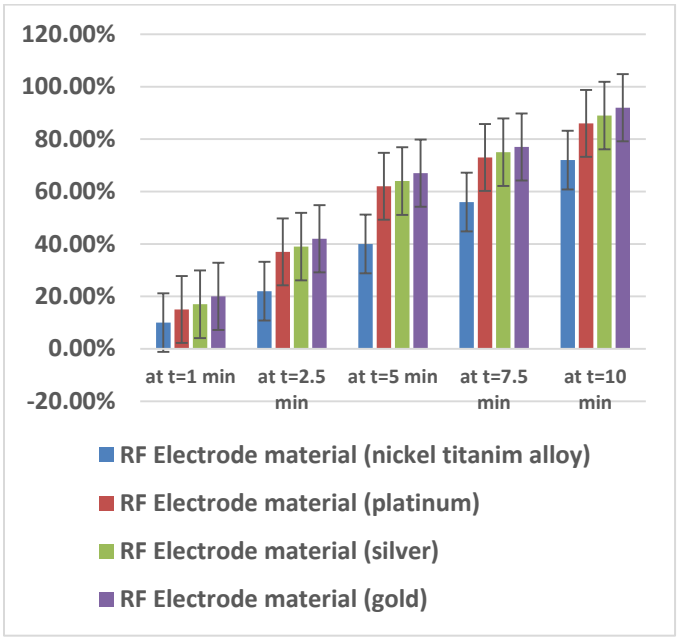

Fig. 8. Comparison of percentage of ablation volume for cool-tip RF electrodes made of Gold, Silver, Platinum, and Nickel-Titanium alloy.

The simulation results and the percentage of ablation achieved from gold, silver, platinum, and nickel-titanium alloy are shown graphically in Fig. 8.

B. Multi-hook RF Electrode

Table III shows the results for the simulations with the new design of multi-hook RF electrode shown in Table III. At the same time and with the same power, there was an appreciable difference in the ablation volume between the different electrode materials.

TABLE III. SIMULATION RESULTS WITH A MULTI-HOOK RF ELECTRODE

Time (min)	Electrode material	Ablation volume(cm^3)
1	Nitinol	2.6
	Pt	4.8
	Ag	6.5
	Au	7.8
2.5	Nitinol	4
	Pt	6..9
	Ag	8.5
	Au	9.8
5	Nitinol	5.3
	Pt	8.5
	Ag	10.2
	Au	11.7
7.5	Nitinol	6.5
	Pt	10.6
	Ag	12.4
	Au	13.5
10	Nitinol	7.9
	Pt	12.3
	Ag	14.3
	Au	15.4

The ablation volume of tumor results output from gold, silver, platinum, and nickel-titanium alloy RF electrodes, respectively, is shown in Fig. 9, 10, 11, and 12, respectively.

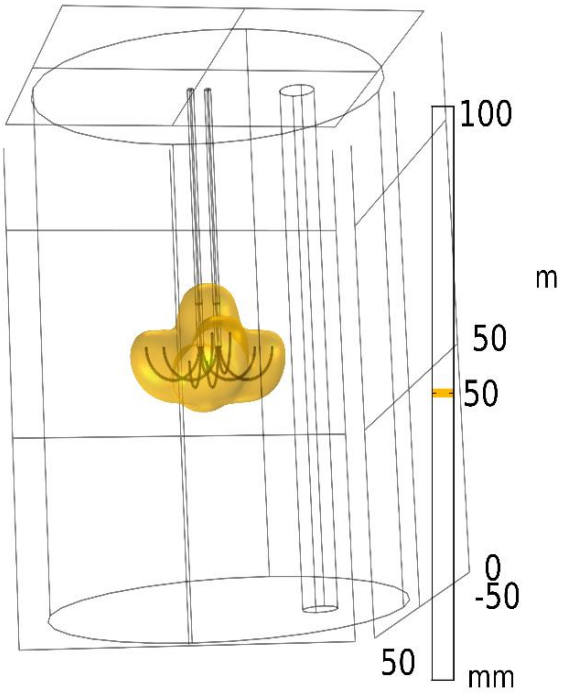

Fig. 9. View of temperature distribution and the ablation volume resulting from using a multi-hook RF electrode made of Gold after ten minutes.

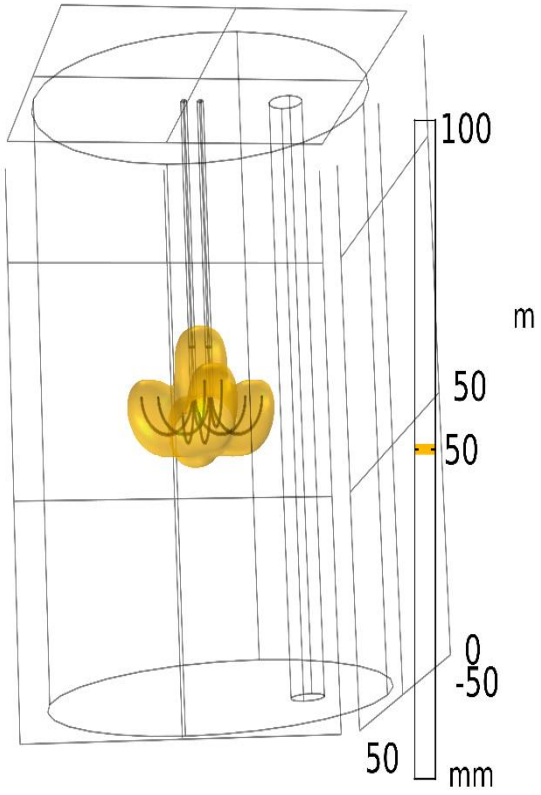

Fig. 10. View of temperature distribution and the ablation volume resulting from using a multi-hook RF electrode made of Silver after ten minutes.

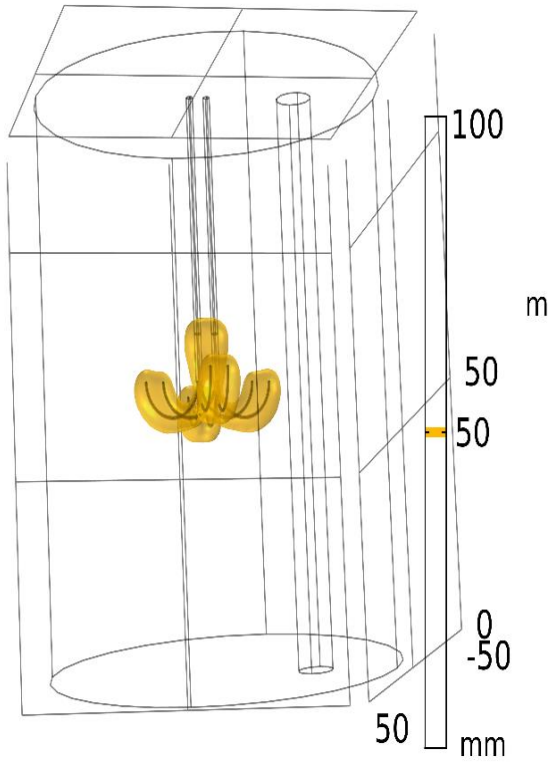

Fig. 11. View of temperature distribution and the ablation volume resulting from using a multi-hook RF electrode made of Platinum after ten minutes.

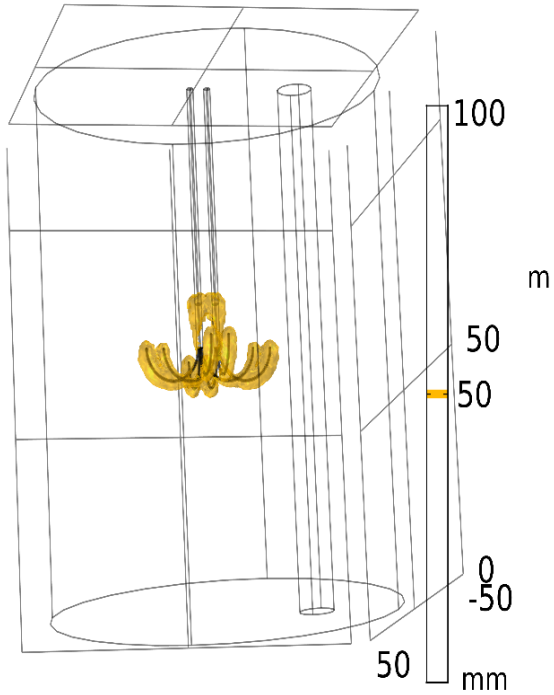

Fig. 12. View of temperature distribution and the ablation volume resulting from using a multi-hook electrode made of Nickel-Titanium alloy after ten minutes.

The simulation results and the percentage of ablation achieved from gold, silver, platinum, and nickel-titanium alloy are shown graphically in Fig. 13.

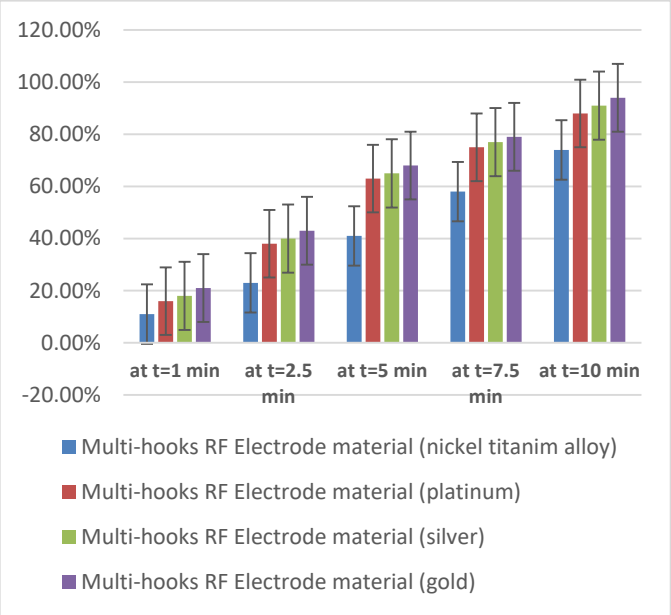

Fig. 13. Comparison of percentage of ablation volume for multi-hook RF electrodes made of Gold, Silver, Platinum, and Nickel-Titanium alloy.

In this paper, we designed a computer model to investigate whether gold, silver, and platinum RF electrodes create larger volume ablation than nickel-titanium alloy electrodes using the same conditions. As shown from the results, for RF and multi-hook electrodes, there is a difference in the percentage of ablation using RF electrodes made of gold, silver, and platinum materials compared to using an electrode made of a nickel-titanium alloy by an amount ranging from five percent to ten percent after a minute, while the difference in the percentage of ablation ranged from 14% to 30%. On the other hand, the ablation rate with the multi-hook electrode is 2% greater than the ablation rate with the cool-tip RF electrode in all kinds of materials used as the multi-hook electrode covers a larger area due to the design difference between the two electrodes.

Previous theoretical research looked into the impacts of using Pt, Ag, and Au as the electrode material for RF ablation rather than nitinol since these metals have higher thermal and electrical conductivities. According to the results, a different amount of ablation was produced, with each of the four electrode materials. Using varied powers at various intervals, we investigated in this study whether Pt, Ag, and Au electrodes produced thermal ablation more successfully than nitinol electrodes. In all simulations, we proved that as the temperature rose, more power was given via the Pt, Ag, and Au electrodes, leading to greater maximum tissue temperatures and a larger ablation volume, as depicted in Fig. 14, 15, and 16. We discovered that the four electrodes' ablation volumes varied.

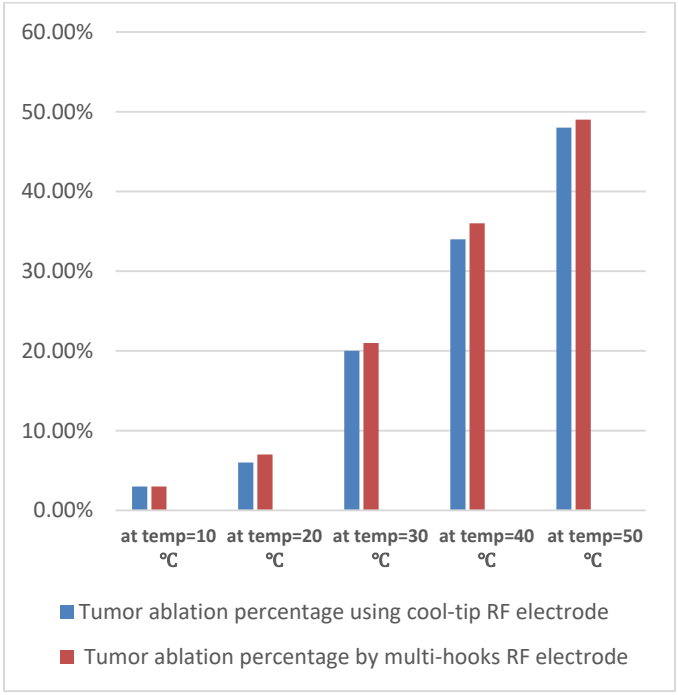

(A)

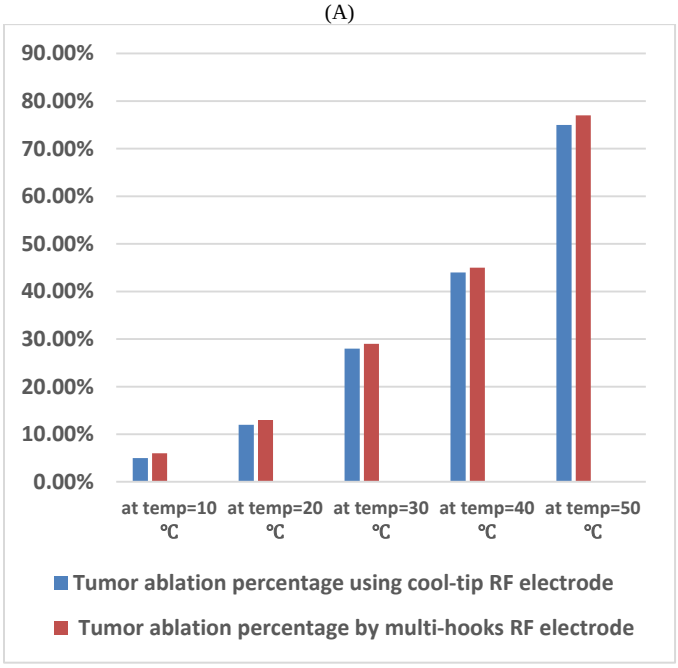

(B)

Fig. 14. Comparison of the percentage of ablation volume for cool-tip and multi-hook RF electrodes, (A) made of Nitinol, and (B) made of Platinum.

Therefore, differences in the thermal and electrical conductivities of RF electrode material offer solutions in certain clinical situations. Our modelling succeeded in reducing time and reducing patient pain.

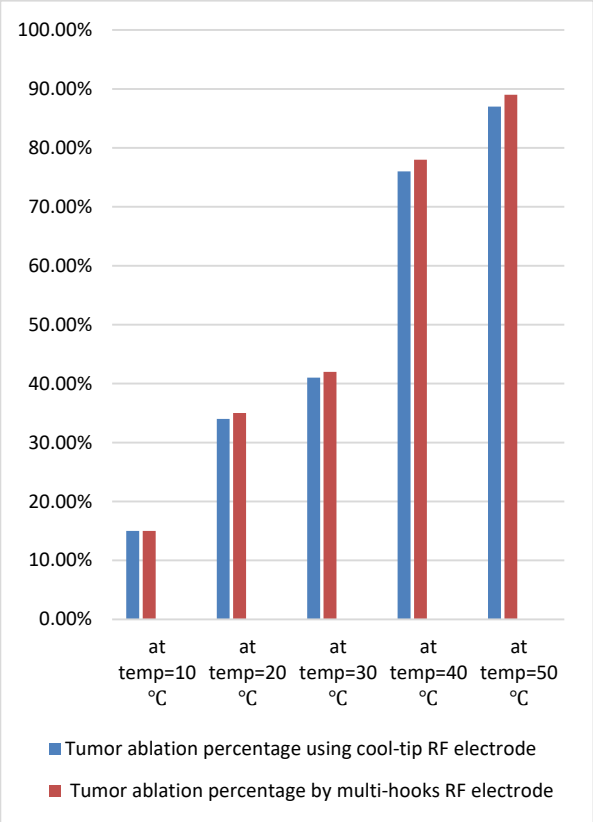

Fig. 15. Comparison of the percentage of ablation volume for cool-tip and multi-hook RF electrodes made of Silver.

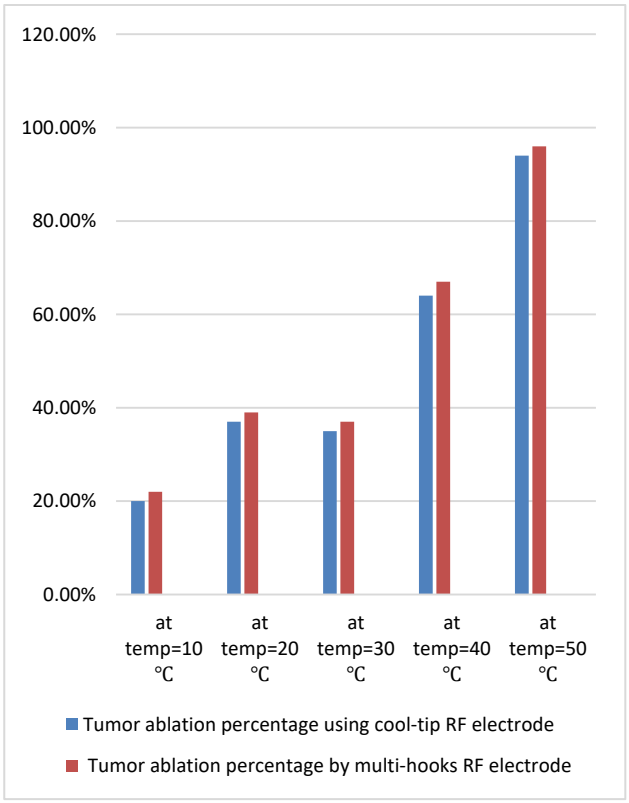

Fig. 16. Comparison of the percentage of ablation volume for cool-tip and multi-hook RF electrodes made of Gold.

IV. Conclusion

The results show that using gamma titanium instead of nickel-titanium achieved an increase in the ablation volume because it has higher electrical and thermal conductivity than nickel-titanium alloy. Also, the results show the effect of tuning parameters (ablation power, ablation time and design of the electrode) on increasing the ablation volume and decreasing the ablation time. The results show that the electrode design is the most important tuning parameter because with the change of design from the reference model to our developed model, the effect and success of the rest of the tunning parameters appeared. That helps to reduce the patient's pain and increase the accuracy. Future work can study the effect of the RF multi-hooks electrodes on large tumors by using the same tuning parameters and compare it with a RF cool-tip electrode.

References

[1] Ferlay, J., et al., Cancer statistics for the year 2020: An overview. International Journal of Cancer, 2021. 149(4): p. 778-789.

[2] Rashed, W.M., et al., Hepatocellular Carcinoma (HCC) in Egypt: A comprehensive overview. Journal of the Egyptian National Cancer Institute, 2020. 32(1): p. 1-11.

[3] Cao, W., et al., Changing profiles of cancer burden worldwide and in China: a secondary analysis of the global cancer statistics 2020. Chinese Medical Journal, 2021. 134(07): p. 783-791.

[4] Sun, Q., et al., Survival analysis following microwave ablation or surgical resection in patients with hepatocellular carcinoma conforming to the Milan criteria. Oncology Letters, 2020. 19(6): p. 4066-4076.

[5] Jarosova, J., et al., Endoscopic radiofrequency ablation for malignant biliary obstruction. World Journal of Gastrointestinal Oncology, 2021. 13(10): p. 1383.

[6] Khattab, A., Regional distribution of lung ventilation during high-frequency jet ventilation in anesthetized patients. 2022, Wien.

[7] Ghosh, R., Computational Modelling and Simulation of RF Induced Heating of Biological Tissue. 2020, State University of New York at Buffalo.

[8] Chen, Q., Model-Based pre-operational plan optimization of hepatic tumor radiofrequency ablation. 2015: Northeastern University.

[9] Lee, M.W., et al., Updated 10-year outcomes of percutaneous radiofrequency ablation as first-line therapy for single hepatocellular carcinoma< 3 cm: emphasis on association of local tumor progression and overall survival. European radiology, 2020. 30(4): p. 2391-2400.

[10] Kim, N., et al., Retrospective analysis of stereotactic body radiation therapy efficacy over radiofrequency ablation for hepatocellular carcinoma. Radiotherapy and Oncology, 2019. 131: p. 81-87.

[11] Fang, Z., et al., Design of a novel electrode of radiofrequency ablation for large tumors: A finite element study. Journal of Engineering and Science in Medical Diagnostics and Therapy, 2018. 1(1).

[12] Rossmann, C. and D. Haemmerich, Review of temperature dependence of thermal properties, dielectric properties, and perfusion of biological tissues at hyperthermic and ablation temperatures. Critical Reviews™ in Biomedical Engineering, 2014. 42(6).

[13] Chang, I., Finite element analysis of hepatic radiofrequency ablation probes using temperature-dependent electrical conductivity. Biomedical engineering online, 2003. 2(1): p. 1-18.

[14] Eliaz, N., Corrosion of metallic biomaterials: A review. Materials, 2019. 12(3): p. 407.

[15] Jagota, V., A.P.S. Sethi, and K. Kumar, Finite element method: an overview. Walailak Journal of Science and Technology (WJST), 2013. 10(1): p. 1-8.

[16] Toyohara, R., et al., Finite element analysis of load transition on sacroiliac joint during bipedal walking. Scientific reports, 2020. 10(1): p. 1-10.

[17] Alemayehu, D.-B. and Y.-R. Jeng, Three-dimensional finite element investigation into effects of implant thread design and loading rate on stress distribution in dental implants and anisotropic bone. Materials, 2021. 14(22): p. 6974.

[18] Segura Félix, K., et al., Computational FEM Model and Phantom Validation of Microwave Ablation for Segmental Microcalcifications in Breasts Using a Coaxial Double-Slot Antenna. BioMed Research International, 2021. 2021.

[19] Mulier, S., et al., Radiofrequency ablation with four electrodes as a building block for matrix radiofrequency ablation: Ex vivo liver experiments and finite element method modelling. Influence of electric and activation mode on coagulation size and geometry. Surgical Oncology, 2020. 33: p. 145-157.

[20] Singh, S. and R. Repaka, Numerical study to establish relationship between coagulation volume and target tip temperature during temperature-controlled radiofrequency ablation. Electromagnetic biology and medicine, 2018. 37(1): p. 13-22.

[21] Mertyna, P., et al., Radiofrequency ablation: the effect of distance and baseline temperature on thermal dose required for coagulation. International journal of hyperthermia, 2008. 24(7): p. 550-559.

[22] Zorbas, G. and T. Samaras, Simulation of radiofrequency ablation in real human anatomy. International Journal of Hyperthermia, 2014. 30(8): p. 570-578.

[23] Singh, S. and R. Repaka, Quantification of thermal injury to the healthy tissue due to imperfect electrode placements during radiofrequency ablation of breast tumor. Journal of Engineering and Science in Medical Diagnostics and Therapy, 2018. 1(1).

[24] Diebold, A., et al., Electrowetting-actuated liquid metal for RF applications. Journal of Micromechanics and Microengineering, 2017. 27(2): p. 025010.

[25] Zhao, P., et al., RF Performance Benchmarking of TSV Integrated Surface Electrode Ion Trap for Quantum Computing. IEEE Transactions on Components, Packaging and Manufacturing Technology, 2021. 11(11): p. 1856-1863.

[26] Safavi, A. and M. Tohidi, Microwave-assisted synthesis of gold, silver, platinum and palladium nanostructures and their use in electrocatalytic applications. Journal of Nanoscience and Nanotechnology, 2014. 14(9): p. 7189-7198.

[27] Pruneanu, S., et al., Electro-catalytic properties of graphene composites containing gold or silver nanoparticles. Electrochimica Acta, 2013. 89: p. 246-252.

[28] Yamada, M., M. Foote, and T.W. Prow, Therapeutic gold, silver, and platinum nanoparticles. Wiley Interdisciplinary Reviews: Nanomedicine and Nanobiotechnology, 2015. 7(3): p. 428-445.

[29] Im, C. and J.-M. Seo, A review of electrodes for the electrical brain signal recording. Biomedical Engineering Letters, 2016. 6(3): p. 104-112.

[30] Kumph, M., et al., Operation of a planar-electrode ion-trap array with adjustable RF electrodes. New Journal of Physics, 2016. 18(2): p. 023047.

[31] Multiphysics, C. COMSOL Multiphysics® 5.4. COMSOL Multiphysics. 2021; Available from: https://www.comsol.com/.

[32] Xu, L., et al., Simulation of multi-probe radiofrequency ablation guided by optical surgery navigation system under different active modes. Computer Assisted Surgery, 2016. 21(1): p. 107-116.

[33] Mahnič-Kalamiza, S. and D. Miklavčič, Scratching the electrode surface: Insights into a high-voltage pulsed-field application from in vitro & in silico studies in indifferent fluid. Electrochimica Acta, 2020. 363: p. 137187.

[34] Attia, M.S., et al., A new method for early diagnosis of liver cancer using a biosensor embedded in an alginate polymer thin film. Journal of Materials Chemistry C, 2022. 10(16): p. 6464-6472.

[35] Ng, E. and M. Jamil, Parametric sensitivity analysis of radiofrequency ablation with efficient experimental design. International journal of thermal sciences, 2014. 80: p. 41-47.

[36] Liang, C., et al., Modeling and analysis of thermal characteristics of magnetic coupler for wireless electric vehicle charging system. IEEE Access, 2020. 8: p. 173177-173185.

[37] Zhang, C., et al., Coupled mechanical-electrical-thermal modeling for short-circuit prediction in a lithium-ion cell under mechanical abuse. Journal of Power Sources, 2015. 290: p. 102-113.

[38] Nonneman, J., et al. Quality Assessment of a 2D FE Based Lumped Parameter Electric Motor Thermal Model Using 3D FE Models. in 2020 International Conference on Electrical Machines (ICEM). 2020. IEEE.

[39] Mi, Y., et al., Multi-parametric study of temperature and thermal damage of tumor exposed to high-frequency nanosecond-pulsed electric fields based on finite element simulation. Medical & biological engineering & computing, 2017. 55(7): p. 1109-1122.

[40] Ghazanfarian, J., R. Saghatchi, and D. Patil, Implementation of smoothed-particle hydrodynamics for non-linear Pennes' bioheat transfer equation. Applied Mathematics and Computation, 2015. 259: p. 21-31.